International Journal of Nanomedicine

Dovepress
open access to scientific and medical research

Open Access Full Text Article

ORIGINAL RESEARCH

Protective Effects of Radix Sophorae Flavescentis Carbonisata-Based Carbon Dots Against Ethanol-Induced Acute Gastric Ulcer in Rats: Anti-Inflammatory and Antioxidant Activities

This article was published in the following Dove Press journal:
International Journal of Nanomedicine

Jie Hu,[1,*] Juan Luo,[1,*] Meiling Zhang,[1] Jiashu Wu,[1] Yue Zhang,[2] Hui Kong,[1] Huihua Qu,[3] Guoliang Cheng,[4] Yan Zhao[1]

[1]School of Traditional Chinese Medicine, Beijing University of Chinese Medicine, Beijing, 100029, People's Republic of China; [2]School of Life Science, Beijing University of Chinese Medicine, Beijing, 100029, People's Republic of China; [3]Center of Scientific Experiment, Beijing University of Chinese Medicine, Beijing, 100029, People's Republic of China; [4]State Key Laboratory of Generic Manufacture Technology of Chinese Traditional Medicine, Lunan Pharmaceutical Group Co., Ltd., Linyi, 276000, People's Republic of China

*These authors contributed equally to this work

Correspondence: Yan Zhao
School of Traditional Chinese Medicine, Beijing University of Chinese Medicine, No. 11 Bei San Huan Dong Lu, Chaoyang District, Beijing, 100029, People's Republic of China
Tel +86 010-62486705
Email zhaoyandr@bucm.edu.cn

Guoliang Cheng
State Key Laboratory of Generic Manufacture Technology of Chinese Traditional Medicine, Lunan Pharmaceutical Group Co., Ltd., No. 209 Hong Qi Lu, Lanshan District, Linyi, 276000, Shandong Province, People's Republic of China
Tel +86 18905391156
Email 18905391156@163.com

Aim: To explore the effects of Radix Sophorae Flavescentis carbonisata-based carbon dots (RSFC-CDs) on an ethanol-induced acute gastric ulcer rat model.

Methods: The structure, optical properties, functional groups and elemental composition of RSFC-CDs synthesized by one-step pyrolysis were characterized. The gastric protective effects of RSFC-CDs were evaluated and confirmed by applying a rat model of ethanol-induced acute gastric ulcers. The underlying mechanisms were investigated through the nuclear factor-kappa B (NF-κB) signalling pathway and oxidative stress.

Results: RSFC-CDs with a diameter ranging from 2–3 nm mainly showed gastric protective effects by reducing the levels of NF-κB, tumour necrosis factor-α (TNF-α), interleukin (IL)-6, superoxide dismutase (SOD), catalase (CAT), glutathione peroxidase (GSH-Px), glutathione (GSH), malondialdehyde (MDA) and inducible nitric oxide synthase (iNOS) to inhibit ethanol-induced inflammation and oxidative stress.

Conclusion: RSFC-CDs have anti-inflammatory and anti-oxidative effects, making them promising for application in ethanol-induced gastric injury.

Keywords: carbon dots, Radix Sophorae Flavescentis, gastroprotection, anti-inflammatory, antioxidant

Introduction

Carbon dots (CDs), a kind of carbon-based zero-dimensional fluorescent nanomaterial with many diverse organic functional groups, have stimulated broad and instructive studies in nanomedicine, including gene/drug delivery,[1] bioimaging,[2] antibacterial agents,[3] and phototherapy,[4] owing to their non/low toxicity, biocompatibility, tunable chemical/optical properties, photostability, and excellent water dispersibility. Recently, the self-bioactivities of CDs have attracted much attention. In particular, the bacteriostat,[5–8] antitumour,[9] free radical scavenging action,[10] anti-inflammation,[11] anti-gout effects,[12,13] haemostasis,[14] hypoglycaemic bioactivity[15] and analgesia[16] effects of CDs have been widely investigated. Although there are many studies on the functions and applications of CDs, research focusing on CDs in Chinese herbal medicine is relatively scarce.

As an effective Chinese herb that has been widely used for more than 2000 years in China, Radix Sophorae Flavescentis (RSF), the dried root of *Sophora*

flavescens Ait., was first recorded in Shen Nong's Classic of the Materia Medica written in the Han Dynasty (202 BC–220 AD) and acknowledged in the Pharmacopoeia of the People's Republic of China (1953). Radix Sophorae Flavescentis Carbonisata (RSFC), the product of RSF prepared by a carbonizing process, has been widely used to treat a multitude of ulcerative diseases throughout the body. Despite abundant clinical reports on the efficacy of RSFC, research on its material basis and the underlying mechanisms is rare.

Gastric ulcers, a common clinical gastrointestinal presentation associated with increased oxidative stress and inflammation, break the mucosal barrier of the stomach lining; susceptibility to ulcers is increased by damaging factors, including smoking, nonsteroidal anti-inflammatory drug (NSAID) medications, alcohol, and *Helicobacter pylori* infection.[17] If not treated sufficiently, gastric ulcers can cause serious complications, such as bleeding and perforation.[18] Even though a variety of drugs are used to treat gastric ulcers, including proton pump inhibitors, antacids, gastric mucosal protectors, and antibiotics, these treatments may cause undesirable side effects and cannot efficaciously control the recurrence of ulcers.[19–21] While some studies focus on the anti-ulcer activity of nanoparticles,[22,23] research on the anti-gastric ulcer activity of CDs in the Chinese Materia Medica is still lacking.

In this study, we prepared fluorescent RSFC-based CDs (RSFC-CDs) by an environmentally friendly, one-step pyrolysis method; characterized the physicochemical properties of the as-prepared RSFC-CDs; and identified the anti-ulcer activity of RSFC-CDs in an ethanol-induced acute gastric ulcer rat model. The underlying mechanisms of the anti-inflammatory and antioxidative stress effects were explored by detecting the levels of NF-κB, TNF-α, IL-6, SOD, CAT, GSH-Px, GSH, MDA and iNOS.

Materials and Methods

Chemicals

RSF was purchased from Beijing Qiancao Herbal Pieces Co., Ltd. (Beijing, China), and the RSFC was prepared in a muffle furnace in our laboratory. Cell Counting Kit-8 (CCK-8) was purchased from Dojindo Molecular Technologies, Inc. (Kumamoto, Japan). Dulbecco's Modified Eagle Medium (DMEM) and foetal bovine serum (FBS) were purchased from Thermo Fisher Scientific Inc. (Waltham, MA, USA). Dialysis membranes with a 1000 Dalton molecular weight cut-off were purchased from Beijing Ruida Henghui Technology Development Co., Ltd. (Beijing, China). SOD, CAT, GSH-Px, GSH, MDA and iNOS kits were purchased from Nanjing Jiancheng Bioengineering Institute of China (Nanjing, China). Rat Enzyme-Linked Immunosorbent Assay (ELISA) kits for NF-κB, TNF-α, and IL-6 were purchased from Cloud-Clone Corp. (Wuhan, China). All other analytical grade chemicals and reagents were purchased from Sino-pharm Chemical Reagents Beijing (Beijing, China).

Animals

Male adult Sprague Dawley (SD) rats of average weight, 220 grams, were purchased from SiPeiFu Biotechnology Co., Ltd. (Beijing, China) and were housed in the Laboratory Animal Center of Beijing University of Chinese Medicine at 24.0 ± 1.0 °C with 55–65% relative humidity under a 12 h light/dark cycle and allowed to feed *ad libitum*. The protocols for this study complied with the Guide for the Care and Use of Laboratory Animals and were approved by the Animal Ethical Committee of Beijing University of Chinese Medicine (NO. BUCM-4-2019112703-4078).

Preparation of RSFC-CDs

RSFC-CDs were synthesized by the one-step pyrolysis method at high temperature with RSF as the carbon source according to previous reports.[24] Placed in porcelain crucibles with sealed lids, RSF was placed in a muffle furnace (TL0612, Beijing Zhongke Aobo Technology Co., Ltd., Beijing, China) at 350 °C for 1 h. The resulting RSFC was then crushed into small pieces, 20 times distilled water was added, and the RSFC was boiled twice at 100 °C for 1 h each time. After filtering through a 0.22 μm microfiltration membrane and condensation using a rotary evaporator, the decoction solution was dialysed with a dialysis membrane (1000 Daltons molecular weight cut-off) against distilled water for 7 days. The obtained RSFC-CDs solution was stored at 4 °C until further use. The flow-process diagram for this preparation is shown in Figure 1. The synthesis yield (weight-by-weight, in %) was calculated considering the amounts of RSFC-CDs powder after purification and the initial precursors.

Characterization of RSFC-CDs

The morphological features, structural details and atomic lattice fringes of RSFC-CDs were measured using transmission electron microscopy (TEM; Tecnai G220, FEI Company, Hillsboro, OR, USA) and high-resolution TEM (HRTEM; JEN-1230, Japan Electron Optics

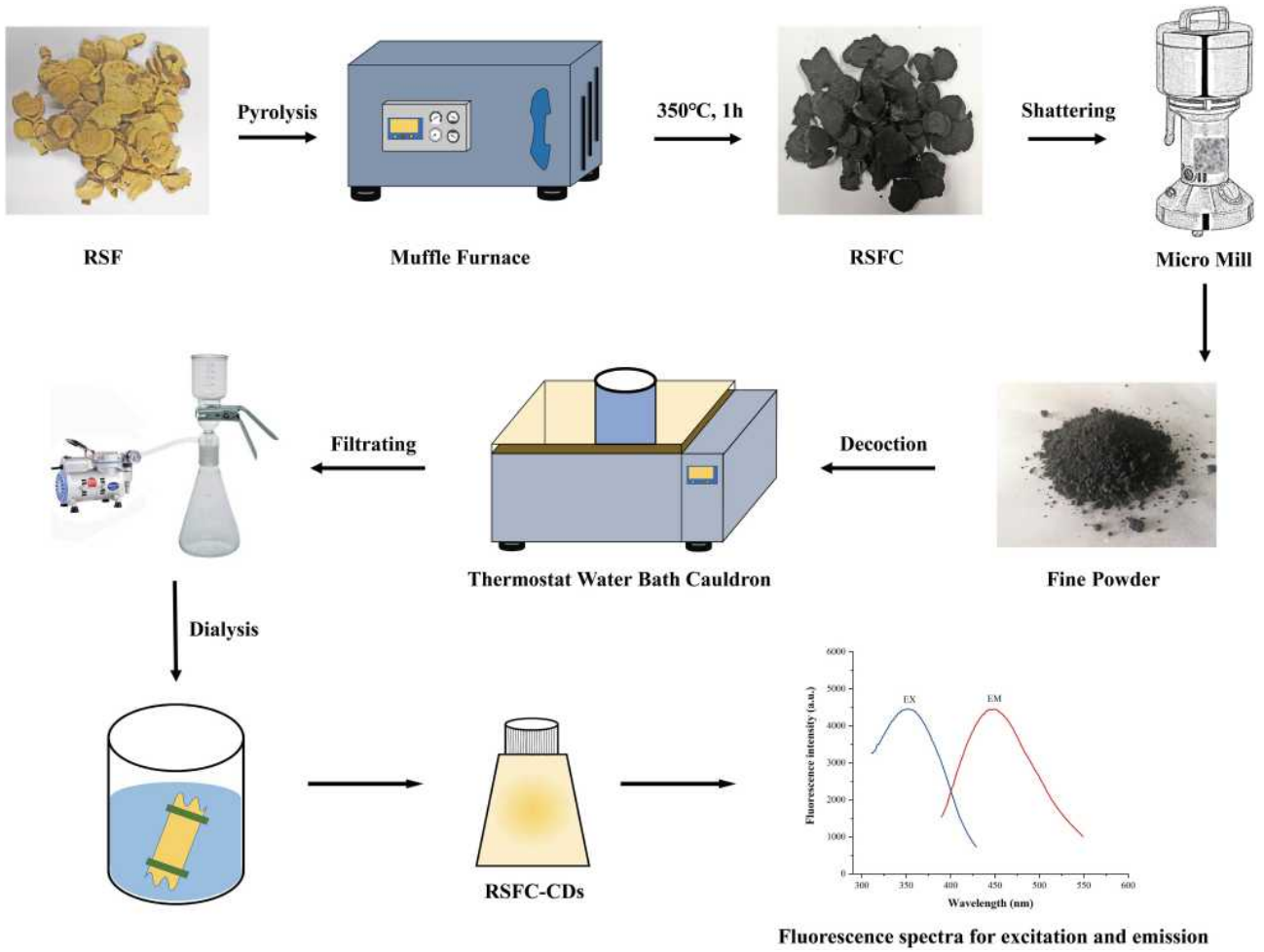

Figure 1 Flow-process diagram of the preparation of Radix Sophorae Flavescentis carbonisata-based carbon dots (RSFC-CDs).

Laboratory, Tokyo, Japan). The X-ray diffraction (XRD) pattern was characterized with a D8 DISCOVER Plus X-ray Diffractometer (Bruker AXS, Karlsruhe, Germany) with Cu K α radiation. The fluorescent performances and ultraviolet-visible (UV-vis) absorption spectra of RSFC-CDs were studied using a fluorescence spectrophotometer (F-4500, Hitachi, Tokyo, Japan) and a UV-vis spectrometer (CECIL, Cambridge, UK). Fourier transform infrared (FTIR) spectroscopy was performed to identify characteristic chemical bonds and functional groups with a FTIR spectrophotometer (Thermo Fisher Scientific, CA, USA). Through X-ray photoelectron spectroscopy (XPS), the surface composition of RSFC-CDs was examined using an X-ray photoelectron spectrometer (ESCALAB 250Xi, Thermo Fisher Scientific, MA, USA) with a mono X-ray source Al Kα 150 W.

Quantum Yield of RSFC-CDs

Applying quinine sulfate (% quantum yield [QY] was 54 in 0.1 M sulfuric acid [H_2SO_4] solution) as a standard sample, the QY of RSFC-CDs was measured using a comparative method and was calculated by the following formula:

$$Q_{CD_S} = Q_R \times \frac{I_{CD_S}}{I_R} \times \frac{A_R}{A_{CD_S}} \times \frac{\eta^2_{CD_S}}{\eta^2_R}$$

where Q represents the QY, I represents the measured integrated emission intensity, and A and η indicate the absorbance at the excitation wavelength and the refractive index of the solvent, respectively. The CDs and the R denote RSFC-CDs and the standard sample, respectively. To minimize the interference of reabsorption, the absorbance of the CDS and the R were kept under 0.05.

Cytotoxicity Assay of RSFC-CDs

The cytotoxicity of the RSFC-CDs on a human gastric epithelial cell line (GES-1 cells) was measured by the CCK-8 kit. GES-1 cells were purchased from Procell Life Science & Technology Co. Ltd. (Wuhan, China). GES-1 cells were cultured in DMEM supplemented with 15% FBS and 1% penicillin-streptomycin (Mediatech, Manassas, VA, USA) and incubated at 37 °C under humidified 5% CO_2. GES-1 cells were seeded in a 96-well plate at a density of 5×10^4 cells per 100 μL/well and cultured for 24 h. The medium in each well was replaced with 100 μL of culture medium containing gradient concentrations (1000, 500, 250, 125, 62.50, 31.25, and 15.63 μg/mL) of RSFC-CDs. After 24 h, the medium containing RSFC-CDs was discarded, and the cells were washed with phosphate-buffered saline (PBS) twice. After adding 10 μL CCK-8 solution per well and incubating for an additional 4 h, the optical density in each well was measured by a microplate reader at 450 nm wavelength. The relative cell viability was calculated using the following formula:

$$\text{Cell viability (\% of control)} = \frac{A_e\text{-}A_b}{A_c\text{-}A_b}\times 100$$

A_e, A_b and A_c denote the absorbance of the experimental, blank and control groups at 450 nm, respectively.

The Ethanol-Induced Damage Model of GES-1 Cells and Drug Treatment

GES-1 cells were cultured under the same conditions and treated with RSFC-CDs of the same gradient concentrations. The medium solution of RSFC-CDs in the 96-well plate was discarded, and the cells were washed with PBS twice. Then, GES-1 cells, except the blank and control groups, were treated with medium containing 5% ethanol and incubated for 3 h. Cells of the blank and control groups were treated with medium containing an equivalent volume of PBS for the same time. Then, the medium containing 5% ethanol was removed, and the cells were washed twice with PBS. Ten microlitres of CCK-8 solution was added to each well, and the solution was incubated for an additional 4 h. Next, the optical density in each well was measured using a microplate reader at a wavelength of 450 nm. The formula is the same as previously described.

The Ethanol-Induced Acute Gastric Ulcer Model in Rats and Drug Treatment

The ethanol-induced acute gastric ulcer model was established by oral administration of ethanol. Male SD rats (n=48) were randomly divided into six groups: the control group (normal saline [NS] 10 mL/kg, p.o.), model group (NS 10 mL/kg, p.o.), positive group (ranitidine 50 mg/kg, p.o.), high group (RSFC-CDs 0.25 mg/kg, p.o.), medium group (RSFC-CDs 0.125 mg/kg, p.o.) and low group (RSFC-CDs 0.0625 mg/kg, p.o.). After 7 days of intervention, rats of all the groups were fasted for 24 h with free access to water. Then, the rats in each group except the control group were given 100% ethanol (5 mL/kg) for 1 h and sacrificed. The blood and stomach were collected to evaluate macroscopic and histopathologic changes.

Evaluation of Ulcer Index and Percentage Inhibition

The stomachs of all rats were removed, cut along the greater gastric curvature, and completely rinsed with ice-cold saline. The total ulcer area was measured using ImageJ software (NIH, Bethesda, MD, USA). The ulcer index (UI) and percentage inhibition were determined using formulas from the literature.[25,26] The UI and percentage inhibition were calculated by the following formulas:

$$\text{Ulcer index (UI)} = \frac{\text{Ulcer partial pixel area}}{\text{Total gastric pixel area}}\times 100\%$$

$$\text{Percentage inhibition} = \frac{\text{UI in model group -UI in each group}}{\text{UI in model group}}\times 100\%$$

Histopathological Evaluation

After observing and taking pictures of gastric tissue, part of the stomach was fixed in a 4% paraformaldehyde solution, dehydrated, embedded in paraffin, sliced into 4–5 μm thick sections, and stained with haematoxylin and eosin (H&E). The stained sections were photographed and observed under a microscope at magnifications of 200× and 400×.

Detection of Relevant Biochemical Indicators in Gastric Tissues

The remaining stomach tissues were rinsed in ice-cold PBS to remove excess blood thoroughly, weighed, cut into small pieces, and homogenized with ice-cold PBS buffer (pH 7.2). Then, the gastric tissue homogenate was centrifuged for 10 min at 3000 rpm to obtain the supernatant to detect the level of oxidative stress (SOD, CAT, GSH-Px, GSH, MDA, and iNOS) by the corresponding kits and inflammatory cytokines (NF-κB, TNF-α, IL-6)

using specific ELISA kits. All the procedures were performed according to the instruction manuals.

Statistical Analysis

Statistical analysis of all experiments was performed using IBM SPSS Statistics (version 20, SPSS Inc., Chicago, IL, USA). The means ± standard deviation (SD) are provided for data with a normal distribution and variance homogeneity. One-way analysis of variance (ANOVA) was performed to compare differences between groups. Data with a non-normal distribution were analysed with nonparametric statistics using the Kruskal–Wallis test with a post hoc test, and $p < 0.05$ and $p < 0.01$ were regarded as statistically significant differences.

Results

Characterization of RSFC-CDs

The morphology and particle size distribution of RSFC-CDs were detected by TEM and HRTEM. The TEM image showed that RSFC-CDs had a practically spherical shape and homogeneous dispersibility with a concentrated size distribution ranging from 2 to 3 nm (Figure 2A and C). The HRTEM image indicated that RSFC-CDs had a graphite-like crystalline framework with a lattice spacing of 0.278 nm (Figure 2B), which was consistent with the (100) planes of graphitic carbon.[27,28] The recognizable diffraction peak (2θ=23.7°) in the XRD pattern (Figure 2D) revealed an amorphous carbon phase of RSFC-CDs, which corresponded with the HRTEM image.[29]

The UV–vis absorption spectrum indicated that RSFC-CDs had an extensive spectrum without any definite peak (Figure 2E). RSFC-CDs exhibited the maximum emission at 449 nm following 352 nm excitation in the fluorescence spectra (Figure 2F). The fluorescence emission spectra of RSFC-CDs under different excitations are shown in Figure 2G. When the wavelength of the excitation light increased from 312 to 512 nm, the emission peaks were all redshifted.

The various surface functional groups of RSFC-CDs were identified based on the FTIR spectra (Figure 2H), which displayed characteristic peaks at 3432 cm^{-1}, 2922 cm^{-1}, 2860 cm^{-1}, 1639 cm^{-1}, 1384 cm^{-1}, and 1058 cm^{-1}. The absorption bands of O-H and N-H stretching vibrations emerged at 3432 cm^{-1}, and the absorption peaks at 2922 cm^{-1} and 2860 cm^{-1} indicated C-H stretching vibrations from $-CH_3$ and $-CH_2$ functional groups, respectively.[30,31] The peak at 1639 cm^{-1} originated from C=O vibrational stretching.[32] A peak appeared at 1384 cm^{-1}, indicating the bending vibrations of C-H and N-H,[33] and the absorption peak at 1058 cm^{-1} was associated with C-O-C stretching vibrations.[34]

The surface element composition and chemical bonds of RSFC-CDs were determined by XPS. The full survey spectrum (Figure 3A) could be divided into three peaks at 284.5, 531.7 and 399.7 eV, which were attributed to C 1s (66.90%), O 1s (26.93%) and N 1s (4.87%), respectively. The high-resolution spectrum of C 1s (Figure 3B) could be deconvoluted into three peaks at 284.1 (C-C/C=C), 285.6 (C-O/C=N) and 287.6 eV (C=O).[35,36] In the high-resolution O 1s spectrum (Figure 3C), two peaks at 530.5 and 531.9 eV were attributed to the presence of O-H and O-C=O bonds, respectively.[37,38] Two peaks at 399.3 and 400.3 eV were in the high-resolution N 1s spectrum (Figure 3D), revealing the existence of pyridinic N and pyrrolic N.[39] The synthesis yield of RSFC-CDs was 3.14 ± 0.2%. The Quantum Yield of RSFC-CDs was 1.08%.

Cytotoxicity Evaluation of RSFC-CDs

To evaluate the cytotoxicity of RSFC-CDs at different concentrations, GES-1 cells were exposed to a series of gradient concentrations of RSFC-CDs ranging from 15.63 to 1000 μg/mL for 24 h (Figure 4A). The results showed that the viability of GES-1 cells was almost 100%, ranging from 15.63 to 250 μg/mL, which was virtually the same as that of the control group. RSFC-CDs at concentrations ranging from 500 to 1000 μg/mL can promote the proliferation of GES-1 cells. All the outcomes confirmed that RSFC-CDs possessed good biocompatibility and lower biotoxicity, even up to 1 mg/mL.

Effect of RSFC-CDs on the Ethanol-Induced Damage Model of GES-1 Cells

To explore the protective effect of RSFC-CDs on ethanol-induced damage, GES-1 cells were treated with gradient concentrations of RSFC-CDs ranging from 15.63 to 1000 μg/mL for 24 h and then exposed to 5% ethanol for 3 h (Figure 4B). As the RSFC-CDs concentration increased, the cell viability also increased, which indicated that RSFC-CDs had a dose-dependent protective effect on ethanol-induced damage to GES-1 cells. RSFC-CDs showed an obvious protective effect on the cells, especially at concentrations of 500 and 1000 μg/mL.

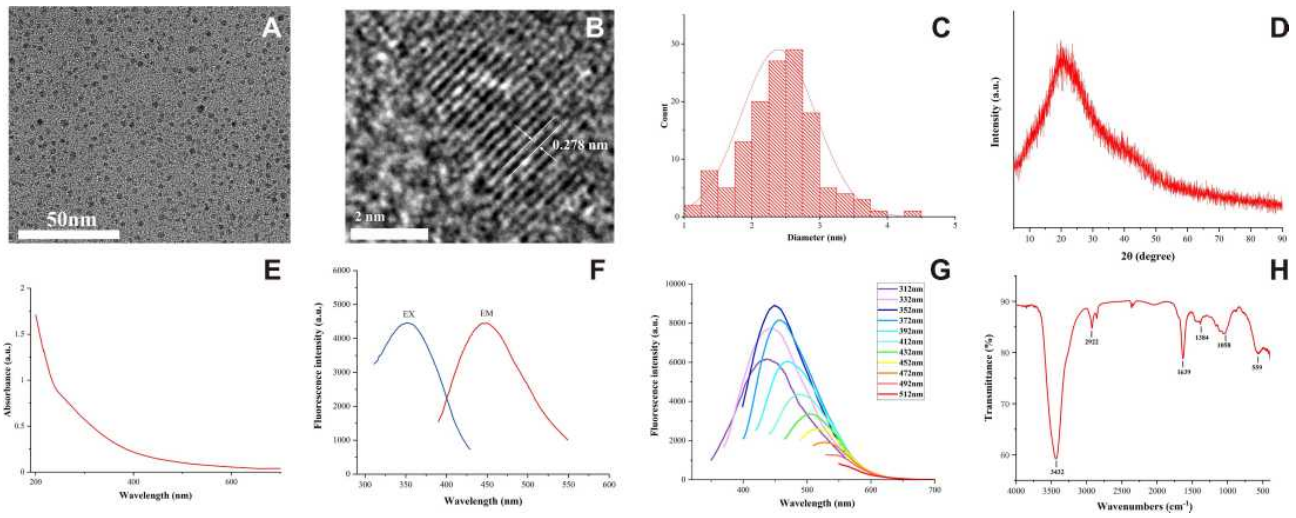

Figure 2 (**A**) Transmission electron microscope (TEM) image of Radix Sophorae Flavescentis carbonisata-based carbon dots (RSFC-CDs). (**B**) High-resolution TEM (HRTEM) image of RSFC-CDs. (**C**) Particle size distribution histogram of RSFC-CDs. (**D**) X-ray diffraction (XRD) pattern of RSFC-CDs. (**E**) Ultraviolet-visible (UV-vis) absorption spectrum of RSFC-CDs. (**F**) Fluorescence spectra for excitation and emission. (**G**) The excitation-dependent fluorescence spectra of RSFC-CDs. (**H**) Fourier transform infrared spectroscopy (FTIR) spectrum of RSFC-CDs.

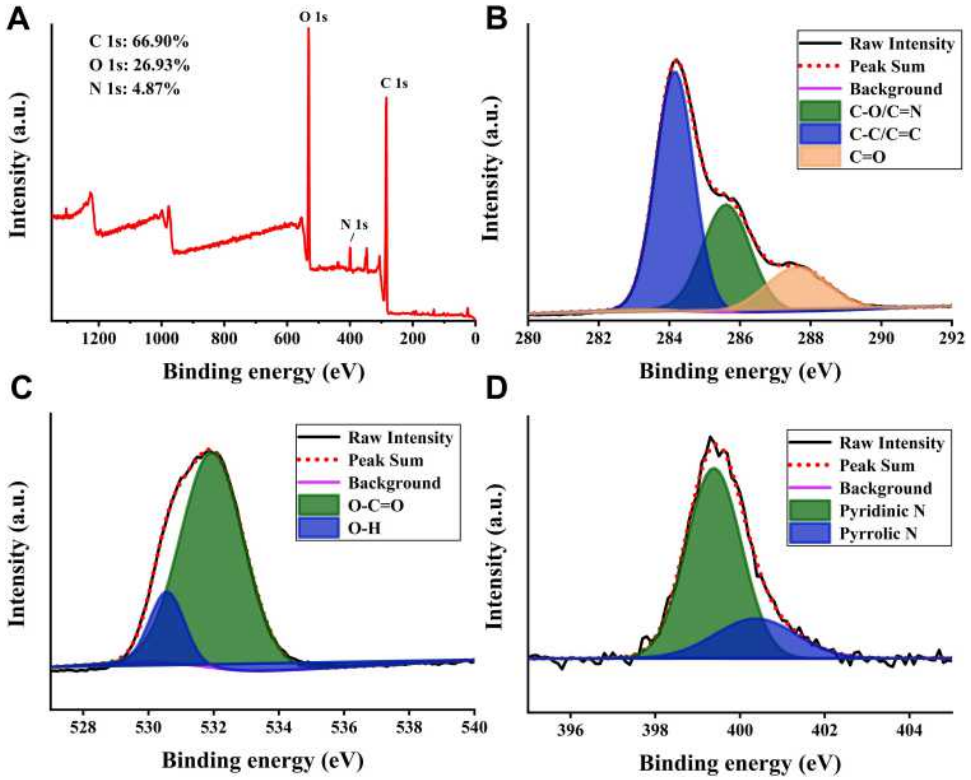

Figure 3 X-ray photoelectron spectroscopy (XPS) spectrum of Radix Sophorae Flavescentis carbonisata-based carbon dots (RSFC-CDs). (**A**) The full survey spectrum. High-resolution survey spectra of (**B**) C 1s, (**C**) O 1s and (**D**) N 1s.

The RSFC-CDs Mitigated Ethanol-Induced Acute Gastric Ulcer in Rats

This study explored the protective effect of RSFC-CDs against acute gastric ulcers in rats induced by oral administration of excessive ethanol, which could lead to mucosal oedema, glandular area hyperaemia, linear haemorrhage necrosis, and multiple other lesions along the long axis of the stomach. In contrast to the control group rats (Figure 5A), rats exposed to ethanol exhibited a broad thick, dull red stripe, which indicated severe haemorrhagic

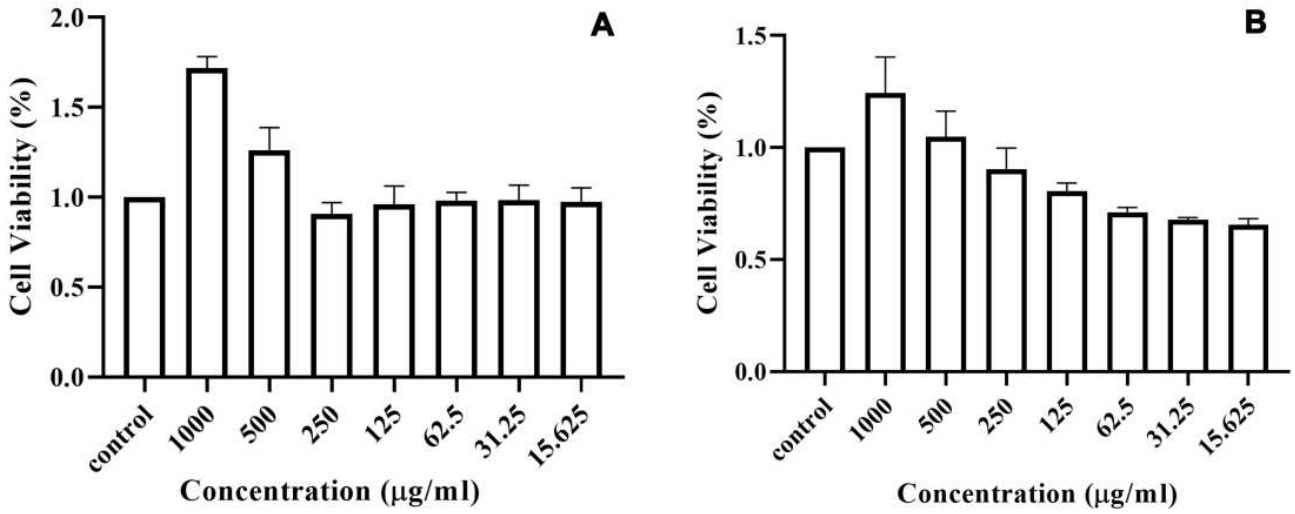

Figure 4 (**A**) Cytotoxicity analysis in GES-1 cells treated with various concentrations of Radix Sophorae Flavescentis carbonisata-based carbon dots (RSFC-CDs). (**B**) The protective effect of different concentrations of RSFC-CDs on the ethanol-induced damage model of GES-1 cells.

lesions of the gastric mucosa. Compared with the model group rats (Figure 5B), animals treated with ranitidine (Figure 5C) and RSFC-CDs (Figure 5D–F) presented lighter, shorter and narrower dull red stripes, which indicated less damage and severity in those groups.

With the purpose of quantifying the changes in the damaged area to evaluate the gastroprotective effect of RSFC-CDs, the ulcer area and percentage inhibition of each group were measured by ImageJ software. The UI (Figure 5G) in the model group (25.87 ± 5.68%) significantly increased, which indicated that the ethanol-induced acute gastric ulcer model was successfully established. All the doses of RSFC-CDs (H: 7.73 ± 0.83%, $p < 0.01$; M: 10.03 ± 0.71%, $p < 0.01$; L: 14.96 ± 1.41%, $p < 0.01$) and ranitidine (5.54 ± 0.58%, $p < 0.01$) significantly decreased the UI. Moreover, the percentage inhibition (Figure 5H) of the positive (78.55 ± 2.24%), high- (70.11 ± 3.21%), medium- (61.20 ± 2.76%), and low- (42.17 ± 5.47%) dose RSFC-CDs groups significantly increased compared with the model group ($p < 0.01$).

RSFC-CDs Ameliorated Ethanol-Induced Gastric Histopathological Damage

The histopathological characterizations of different groups illustrated the microscopic alterations in gastric tissues, revealing ethanol-induced damage and the protective bioactivity of RSFC-CDs (Figure 6). It can be seen clearly from the control group with a normal gastric wall structure that the intact gastric mucosa was flat and smooth and the arrangement of glandular cells was tidy (Figure 6A and D). Ethanol-induced oedema and inflammatory cell infiltration were found in the submucosal area in the model group. Furthermore, severe intervillous haemorrhages were observed; these were associated with severe exfoliation of the mucosal epithelium (Figure 6B and E). In contrast, pretreatment with oral administration of ranitidine (Figure 6C and F) and RSFC-CDs (H: Figure 6G and J; M: Figure 6H and K) significantly ameliorated the exfoliation of mucosal cells, scattered bleeding, oedema, and inflammatory cell infiltration. Additionally, the low-dose group (Figure 6I and L) exhibited a protective tendency against histopathological damage. However, the improvement was relatively more pronounced in the ranitidine group and the RSFC-CDs groups (high- and medium-dose) than in the low-dose group.

RSFC-CDs Mitigated Oxidative Stress by Upregulating the Activity of Antioxidants

Overdose ethanol can stimulate acute gastric injuries mediated by overexpressing reactive oxygen species (ROS). As one of the mechanisms of stimulation, severe oxidative damage is triggered by ROS and plays a vital role in ulcerative and haemorrhagic lesions.[25] The alterations of the redox status were further assessed by the level of antioxidant and peroxidation products. The antioxidant capacity was illustrated through an assessment of enzymatic antioxidant (CAT, SOD, GSH-Px) and non-enzymatic antioxidant (GSH) levels in stomach tissues (Figure 7A–D). The gastric tissue damage caused by oxidative stress was evaluated by the levels of MDA and iNOS (Figure 7E and F).

Ethanol intervention in the model group caused a significant decrease in the activities of CAT (0.65 ± 0.15 U/mgport, $p <$

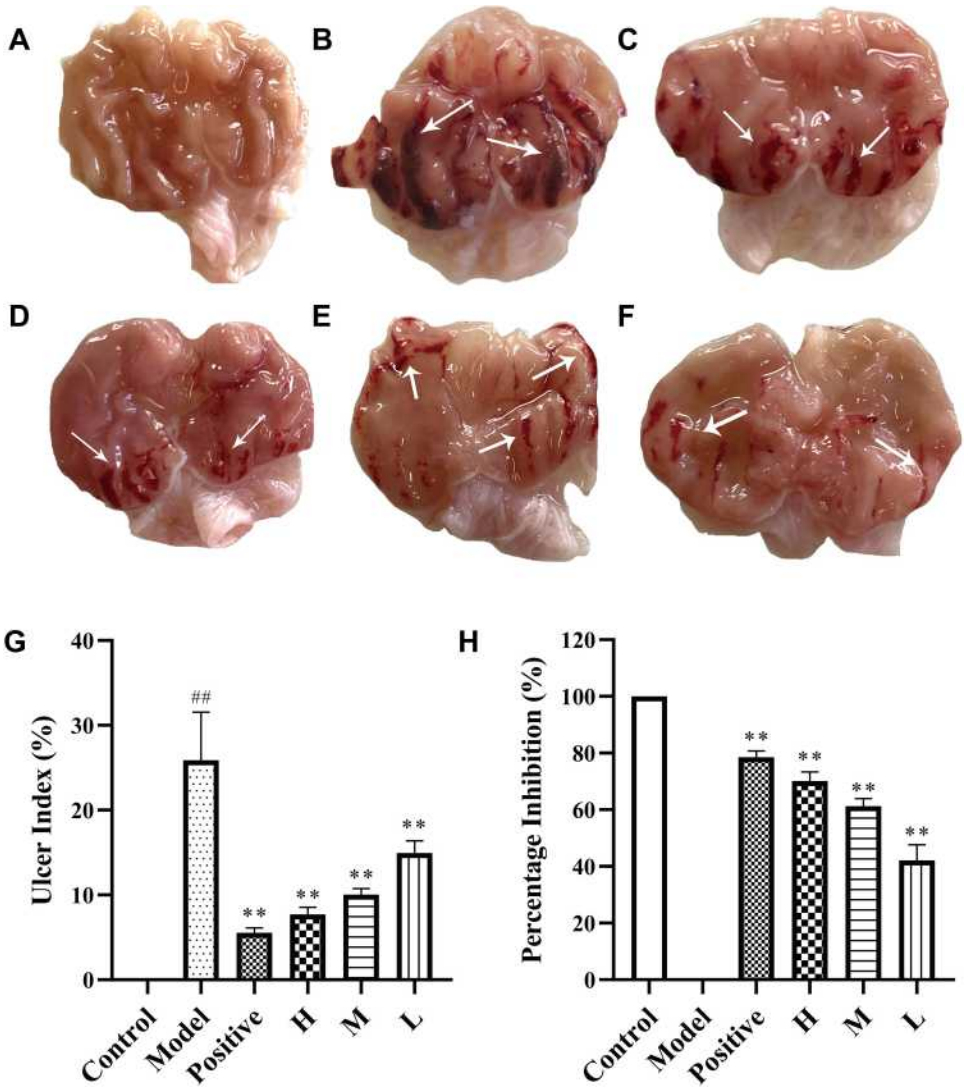

Figure 5 Macroscopic images of Radix Sophorae Flavescentis carbonisata-based carbon dots (RSFC-CDs) ameliorating an ethanol-induced acute gastric mucosal injury. (**A**) Control group. (**B**) Model group. (**C**) Positive group. (**D**) High-dose RSFC-CDs group. (**E**) Medium-dose RSFC-CDs group. (**F**) Low-dose RSFC-CDs group. (**G**) The ulcer index. (**H**) Percentage inhibition of each group. Data are expressed as the mean ± SD. $^{\#\#}p < 0.01$ compared with the control group, $^{**}p < 0.01$ compared with the model group.

0.01), SOD (337.88 ± 32.74 U/mgport, $p < 0.01$), GSH-Px (587.28 ± 12.56 U/mgport, $p < 0.01$), and GSH (0.77 ± 0.11 μmol/gport, $p < 0.01$) compared with the control group (CAT: 1.78 ± 0.28 U/mgport; SOD: 531.30 ± 35.23 U/mgport; GSH-Px: 695.38 ± 25.42 U/mgport; GSH: 1.90 ± 0.33 μmol/gport).

Conversely, pretreatment with high and medium doses of RSFC-CDs produced a significant increase in the levels of CAT (H: 1.28 ± 0.15 U/mgport, $p < 0.01$; M: 1.16 ± 0.07 U/mgport; $p < 0.01$), SOD (H: 443.28 ± 28.35 U/mgport, $p < 0.01$; M: 454.30 ± 33.69 U/mgport, $p < 0.01$), GSH-Px (H: 673.82 ± 26.52 U/mgport, $p < 0.01$; M: 652.91 ± 29.93 U/mgport, $p < 0.05$), and GSH (H: 1.46 ± 0.23 μmol/gport, $p < 0.01$; M: 1.33 ± 0.17 μmol/gport, $p < 0.01$). Moreover, improvements of those antioxidants (CAT: 1.65 ± 0.24 U/mgport, $p < 0.01$; SOD: 469.61 ± 30.15 U/mgport, $p < 0.01$; GSH-Px: 676.02 ± 39.07 U/mgport, $p < 0.05$; GSH: 1.72 ± 0.24 μmol/gport, $p < 0.01$) were more obvious in the group treated with ranitidine. In contrast to the model group, the low dose of RSFC-CDs significantly upregulated the activities of CAT (1.06 ± 0.18 U/mgport; $p < 0.05$) and SOD (425.08 ± 24.37 U/mgport, $p < 0.01$). At the same time, low-dose RSFC-CDs increased the levels of GSH (1.10 ± 0.27 μmol/gport; $p > 0.05$) and GSH-Px (609.49 ± 17.75 U/mgport; $p > 0.05$), but without significant differences.

RSFC-CDs can not only upregulate the level of antioxidants in ethanol-induced gastric injury but also downregulate the levels of lipid peroxide metabolites (MDA) and iNOS to balance the levels of antioxidant and peroxidation

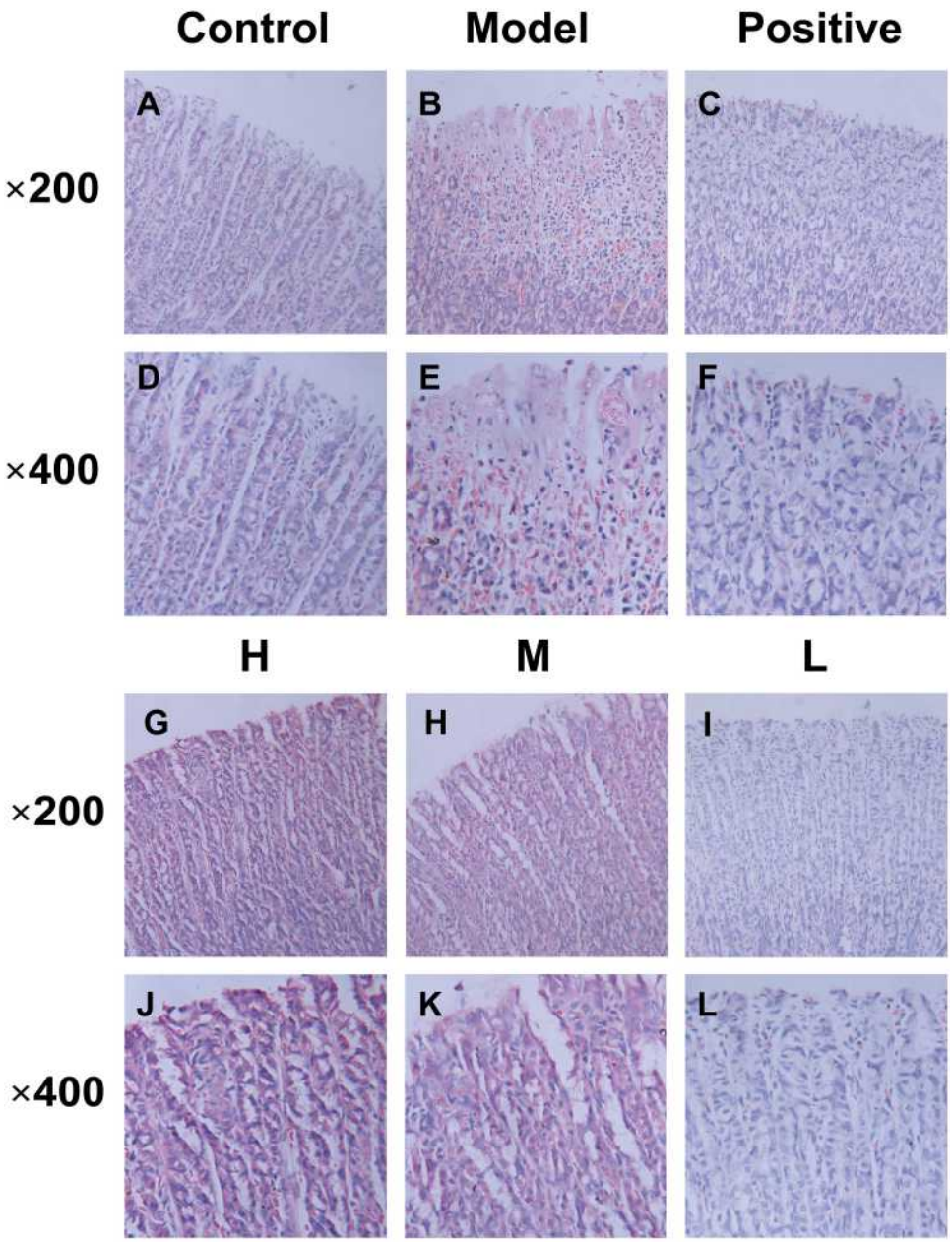

Figure 6 Radix Sophorae Flavescentis carbonisata-based carbon dots (RSFC-CDs) ameliorate ethanol-induced gastric histopathological damage. Histopathological sections of gastric tissue were stained with H&E. The control group (**A** and **D**) illustrated the normal structure of the gastric wall with an intact gastric mucosa. The model group (**B** and **E**) demonstrated the exfoliation of the mucosal epithelium, haemorrhage, oedema, and inflammatory cell infiltration. Positive (**C** and **F**), high-dose (**G** and **J**), medium-dose (**H** and **K**), and low-dose (**I** and **L**) RSFC-CDs groups showed that the gastric injuries had improved to varying degrees.

products. Compared with the control group (MDA: 22.68 ± 3.29 nmol/mgport; iNOS: 3.33 ± 0.65 U/mgport), ethanol caused MDA (69.84 ± 7.18 nmol/mgport, $p < 0.01$) and iNOS (9.51 ± 1.57 U/mgport, $p < 0.01$) to rise significantly. Pretreatment with high and medium doses of RSFC-CDs significantly decreased the levels of MDA (H: 25.65 ± 2.69 nmol/mgport, $p < 0.01$; M: 44.06 ± 7.40 nmol/mgport, $p < 0.01$) and iNOS (H: 4.87 ± 0.42 U/mgport, $p < 0.01$; M: 6.52 ± 1.18 U/mgport, $p < 0.01$). At the same time, administration of the low dose of RSFC-CDs downregulated the levels of MDA (55.75 ± 3.77 nmol/mgport; $p < 0.05$) and iNOS (8.12 ± 0.96 U/mgport; $p > 0.05$).

RSFC-CDs Inhibited TNF-α and IL-6 by Downregulating the Expression of NF-κB

Inflammation is another important underlying mechanism of acute gastric ulcers induced by an overdose of ethanol, which can be activated by the NF-κB pathway and upregulated by its downstream proinflammatory effectors.

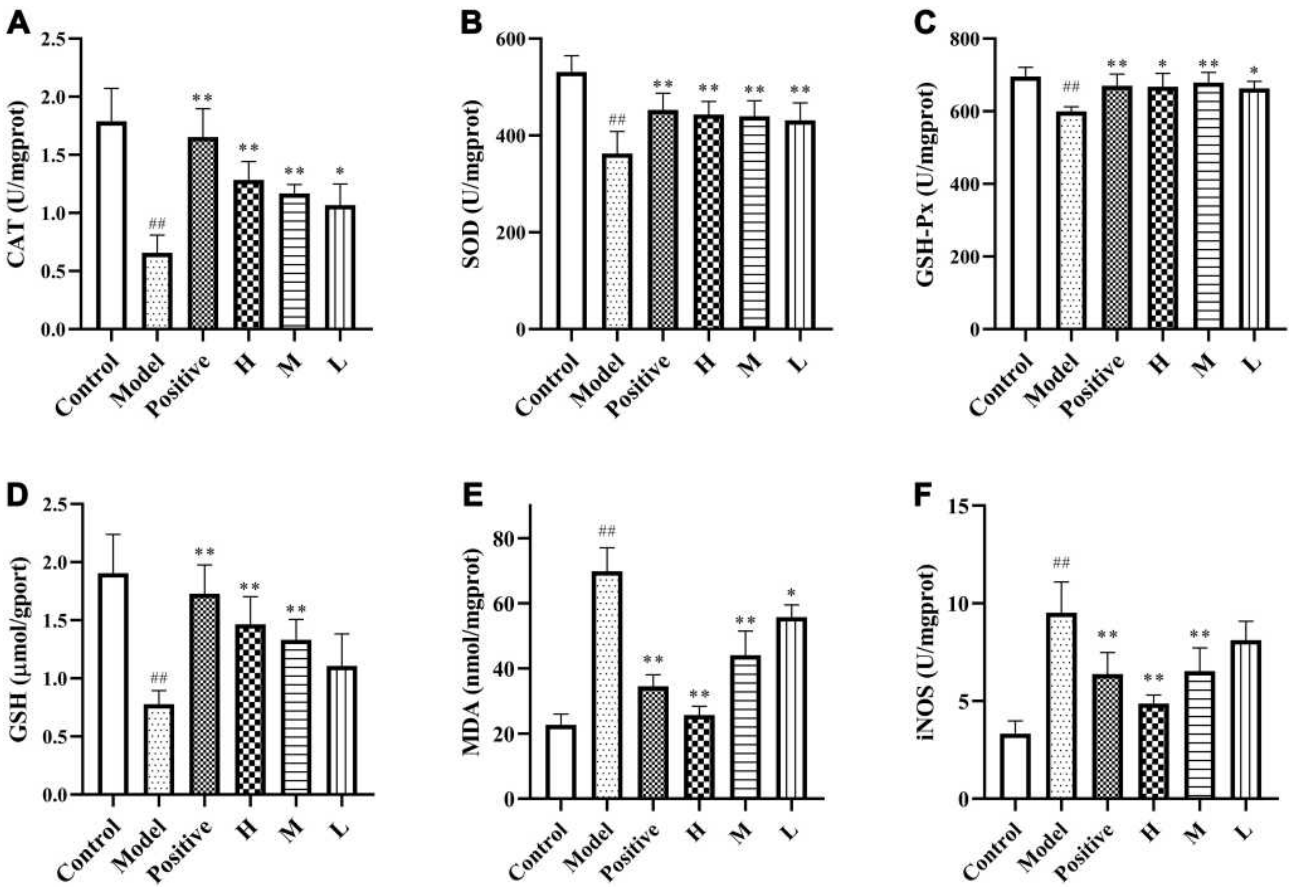

Figure 7 Effects of Radix Sophorae Flavescentis carbonisata-based carbon dots (RSFC-CDs) on the levels of (**A**) catalase (CAT), (**B**) superoxide dismutase (SOD), (**C**) glutathione peroxidase (GSH-Px), (**D**) glutathione (GSH), (**E**) malondialdehyde (MDA) and (**F**) inducible nitric oxide synthase (iNOS) in gastric tissue homogenate supernatant. Data are expressed as the mean ± SD. $^{\#\#}p < 0.01$ compared with the control group, $^{*}p < 0.05$ and $^{**}p < 0.01$ compared with the model group.

When comparing NF-κB in stomach tissue, the level in the model group (1.63 ± 0.19 ng/mL) increased significantly ($p < 0.01$) over that of the control group (0.56 ± 0.06 ng/mL). In the positive (0.80 ± 0.13 ng/mL; $p < 0.01$), high-dose (1.03 ± 0.21 ng/mL; $p < 0.01$) and medium-dose (1.12 ± 0.21 ng/mL; $p < 0.05$) groups, the concentrations of NF-κB decreased significantly in comparison to that in the model group. There was no significant change detected in the low-dose group (1.34 ± 0.14 ng/mL) compared with the model group (Figure 8A).

The TNF-α level in the stomach tissue of the model group (12,992.76 ± 1410.92 pg/mL) was also significantly increased ($p < 0.01$) in comparison to that of the control group (7562.29 ±707.16 pg/mL). The level of TNF-α in the positive (7726.66 ± 982.42 pg/mL; $p < 0.01$), high-dose (7769.58 ± 1678.01 pg/mL; $p < 0.01$), medium-dose (8567.21 ± 1744.45 pg/mL; $p < 0.01$) and low-dose (9722.50 ± 1247.51 pg/mL; $p < 0.05$) groups significantly decreased compared with that in the model group (Figure 8B).

Likewise, the IL-6 level in the stomach tissues of the model group (232.00 ± 29.43 pg/mL) was significantly upregulated ($p < 0.01$) compared with that of the control group (119.53 ±12.43 pg/mL). In comparison to the model group, the IL-6 level of the positive (112.74 ± 18.63 pg/mL), high-dose (120.88 ± 30.98 pg/mL), and medium-dose (123.48 ± 25.85 pg/mL) groups was significantly downregulated ($p < 0.01$). In contrast, there was no significant difference observed in the low-dose group (189.03 ± 19.36 pg/mL) compared to the model group (Figure 8C).

Discussion

CDs have been exploited for biosensing, bioimaging, fluorescent labelling, diagnosis, drug delivery, targeted therapy, and other medical fields[40–43] for their merits of excellent photostability, photobleaching resistance and biocompatibility. Nevertheless, studies focused on the self-bioactivities of CDs are relatively insufficient and may be concerned with carbon sources lacking inherent bioactivities or synthetic

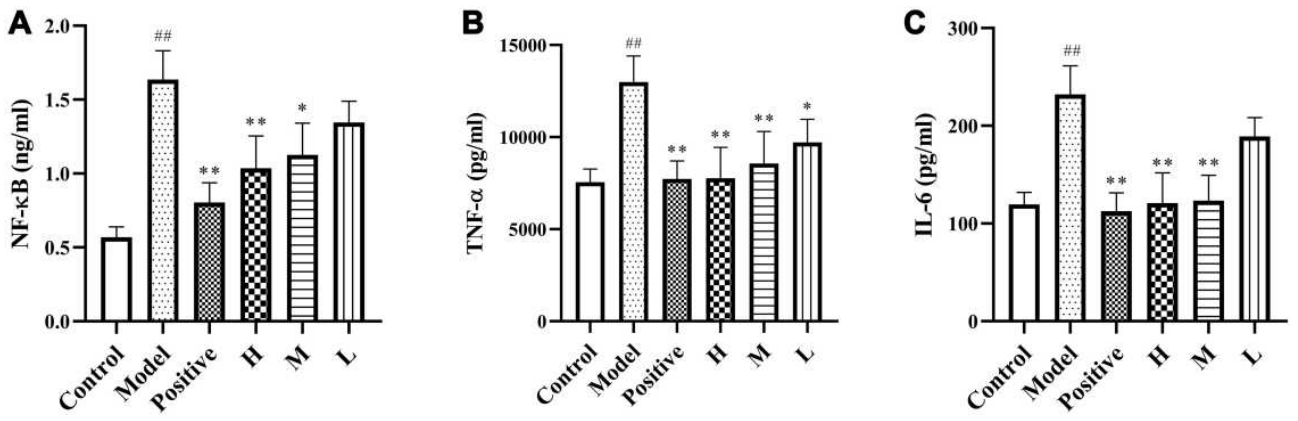

Figure 8 Effects of Radix Sophorae Flavescentis carbonisata-based carbon dots (RSFC-CDs) on the levels of (**A**) nuclear factor-kappa B (NF-κB), (**B**) tumour necrosis factor-α (TNF-α), and (**C**) interleukin (IL)-6 in gastric tissue homogenate supernatant. Data are expressed as the mean ± SD. $^{\#\#}p < 0.01$ compared with the control group, $^{*}p < 0.05$ and $^{**}p < 0.01$ compared with the model group.

conditions.[44] A number of previous studies have identified the innate bioactivities of CDs, such as carbon nanodots from metronidazole possessing selective antibacterial activity against obligate anaerobes,[45] ginsenoside Re-based CDs displaying inhibition efficiency of cancer cells,[44] and Gly-CDs synthesized from glycyrrhizic acid exhibiting excellent antiviral properties.[46] However, CDs with inherent biological activities have immense clinical research potential.

Produced by a high-temperature carbonization process that is similar to high-temperature pyrolysis, a bottom-up synthesis method, a number of charcoal medicines with various functions have been widely used in traditional Chinese medicine for more than 2000 years. Traditional Chinese herbs, as organic carbon sources with superiorities of low cost, low toxicity, moderate reaction, and eco-environmental friendliness, have a variety of clinical treatment effects. It is interesting to note that charcoal medicines and their carbon sources both have conspicuous self-activities, which inspire us to conclude that CDs prepared with traditional Chinese herbs using high-temperature pyrolysis may have inherent bioactivities. Prior studies by our research team revealed that CDs derived from charcoal medicines have various bioactivities as the functional material basis of charcoal medicines. The results indicate that CDs derived from Pollen Typhae,[47] Herba Cirsii Japonici[48] and Phellodendri Cortex[24] have haemostatic bioactivity; CDs derived from Jiaosanxian have hypoglycaemic bioactivity,[15] CDs derived from Junci Medulla have hepatoprotective bioactivity;[49] CDs derived from Lonicerae Japonicae Flos have bioactivities of alleviating fever and hypothermia;[50] CDs derived from Zingiberis Rhizoma have analgesic activity;[16] and CDs derived from Aurantii Fructus Immaturus have antihyperuricaemic and anti-gouty arthritis activities.[13]

This study focused on RSFC, one of the charcoal medicines widely used in ulcerative, haemorrhagic, traumatic and infective diseases. The solution was synthesized from the active precursor RSF, and we evaluated the effects of RSFC-CDs on ethanol-induced acute gastric ulcers in rats and explored the underlying mechanism of anti-inflammatory and anti-oxidative stress. One-step high-temperature pyrolysis was applied due to its cost-effective and eco-friendly synthesis. The as-prepared fluorescent RSFC-CDs with tiny sizes possessed abundant functional groups, which was beneficial for multiple biological activities.

Using GES-1 cells to evaluate the cytotoxicity of the RSFC-CDs and their protective effect on ethanol-induced damage, our results illustrated that the RSFC-CDs had excellent biocompatibility and low toxicity and significantly ameliorated ethanol-induced damage. The RSFC-CDs not only showed an apparent cytoprotective effect but also had a significant protective effect on ethanol-induced gastric ulcer rats both in macrography and micrography. In macroscopic measurements, the RSFC-CDs could effectively allay gastric oedema, hyperaemia, and haemorrhagic necrosis induced by an overdose of ethanol, thereby decreasing the UI and increasing the percentage inhibition. Microscopic measurements showed that the RSFC-CDs could defend the gastric mucosa by lessening exfoliation of the gastric mucosal epithelium, haemorrhage, oedema, and inflammatory infiltration of the stomach.

Gastric ulcers characterized by multiple types of mucosal injuries were induced by various pathogenic factors. As a prominent invasion factor of gastric ulcers, ethanol can quickly and easily penetrate and invade the gastric mucosa and give rise to mucosal injuries or even into the muscularis, which can provoke excessive inflammation, oxidative damage, cell necrosis, and apoptosis of gastric mucosa, as proven by prior studies.[51]

The inflammatory response mediated by the NF-κB signalling pathway plays a crucial role in ethanol-induced acute gastric ulcers. NF-κB induces cytokines that regulate the inflammatory response, which leads to the recruitment of leukocytes to sites of inflammation.[52] Previous research has established that downregulated levels of NF-κB and downstream pro-inflammatory cytokines (ie, TNF-α, IL-6) can ameliorate gastric mucosal injuries generated by an overdose of ethanol.[53–55] In this study, RSFC-CDs downregulated the levels of NF-κB, TNF-α and IL-6 in injured gastric tissues to inhibit further deterioration triggered by an overdose of ethanol, which may be one potential mechanism of gastric protection for RSFC-CDs.

Oxidative damage mediated by over-expressed ROS is another critical mechanism in ethanol-induced acute gastric ulcers. Accumulated and excessive ROS will consume endogenous antioxidants and destroy the internal defensive system, which can cause lipid peroxidation, cellular death, and tissue damage, prompting the aggravation of gastric injury.[56] The NF-κB signalling pathway could be activated by ROS produced within the cell.[57] Numerous studies have described that a decline in antioxidants is relevantly associated with gastric injuries and that heightened antioxidants can lessen the severity of alcohol-induced damage.[54,55,58] These results indicated that the RSFC-CDs could promote the expression of enzymatic antioxidants (CAT, SOD, GSH-Px) and non-enzymatic antioxidants (GSH) in stomach tissues to neutralize the over-expressed oxidant, which could be the underlying mechanism by which RSFC-CDs alleviate gastric lesions. At the same time, RSFC-CDs could downregulate the levels of lipid peroxide metabolites (MDA) and pro-inflammatory mediators (iNOS) to mitigate the degree of damage induced by oxidative stress.

RSFC-CDs exhibited protective effects for curing ethanol-induced acute gastric ulcers with anti-inflammatory and anti-oxidative bioactivities, which may be correlated with their diverse surface functional groups. With diverse surface functional groups, CDs are composed of hybridized sp^2 and sp^3 carbon atoms, which form a core-shell structure.[59,60] CDs are widely studied in medicine and life science research due to their impressive surface properties, although their exact structure has not been completely revealed.[45,46,61,62] The antibacterial property of carbon nanodots synthesized from metronidazole may be primarily attributed to the nitro group.[45] Gly-CDs retained most functional groups of precursors, which could further affect antiviral activity.[46] The characteristic functional groups of ginsenoside still remained on the surface of ginsenoside Re-based CDs, which are probably crucial to its anticancer bioactivity.[44] The acetyl groups retained from aspirin and the amide groups in synthesized FACD exerted synergistic effects, leading to increased anti-inflammatory bioactivities compared to aspirin alone.[63] Similarly, the enhanced anti-inflammatory effect of ibuprofen-based carbon quantum dots might be related to the formation of acetyl groups.[64] All of these previous studies indicate that the various functional groups on the surface of CDs play essential roles in their inherent bioactivities.

Although there are currently several kinds of medicines used for the treatment of upper gastrointestinal ulcers, such as antacids, there are no specific medicines for the treatment of acute gastric ulcers. As the first-line treatment for gastric ulcers, proton pump inhibitors and H_2 receptor blockers can effectively inhibit gastric acid secretion to protect the gastric mucosa.[65] However, these inhibitors also provoke multitudinous serious adverse reactions in clinical applications, such as acute interstitial nephritis,[66] subacute cutaneous lupus erythaematosus,[67] myocardial infarction,[68,69] and hepatic encephalopathy.[70] Hence, exploring a new type of safe and low-toxicity medicine with anti-gastric ulcer effects has attracted the attention of researchers. As the precursor of RSFC-CDs, RSFC, which has a long history of clinical applications, is still applied to treat ulcerative diseases throughout the body due to its remarkable clinical effects. Synthesized via a green method with an extensive precursor source, RSFC-CDs not only display a therapeutic effect comparable to ranitidine but also show no obvious biological toxicity and have outstanding biocompatibility, which indicate that they have tremendous potential as a candidate treatment for gastric ulcers.

The results of this study show that the gastric protective bioactivity of RSFC-CDs is caused by lessening the oxidative damage and inflammatory response provoked by ethanol. This study primarily illustrated the anti-inflammatory and anti-oxidative action of RSFC-CDs through the NF-κB signalling pathway and ROS system. Hence, future research will focus on the comprehensive mechanisms of gastric protection and other bioactivities of RSFC-CDs.

Conclusion

In conclusion, novel fluorescent RSFC-CDs with inherent bioactivity, good biocompatibility, and low toxicity were synthesized by one-step pyrolysis using RSF as the sole precursor. To the best of our knowledge, for the first time, the gastroprotective activity of RSFC-CDs at the molecular, cellular, and animal levels was demonstrated. By decreasing the concentrations of NF-κB and its downstream proinflammatory cytokines (TNF-α and IL-6), the RSFC-CDs inhibited inflammation in gastric tissues. At the same time, the RSFC-CDs increased the levels of CAT, SOD, GSH-Px and GSH and decreased the levels of MDA and iNOS to mitigate the oxidative stress induced by ethanol. These outstanding characteristics make RSFC-CDs a safe and effective nanomedicine that has good potential for applications in the clinical therapy of ethanol-induced gastric injury.

Acknowledgments

This work is supported by the National Natural Science Foundation (grant number 81503344), the Classical Prescription Basic Research Team of the Beijing University of Chinese Medicine (2019-JYB-TD-001), and the Basic Scientific Research Fund of Beijing University of Chinese Medicine (2180072120096).

Disclosure

Guoliang Cheng is an employee of Lunan Pharmaceutical Group Co., Ltd. The authors report no other potential conflicts of interest for this work.

References

1. Jia X, Pei M, Zhao X, Tian K, Zhou T, Liu P. PEGylated oxidized alginate-DOX prodrug conjugate nanoparticles cross-linked with fluorescent carbon dots for tumor theranostics. *ACS Biomater Sci Eng*. 2016;2(9):1641–1648. doi:10.1021/acsbiomaterials.6b00443
2. Zhao N, Wang Y, Hou S, Zhao L. Functionalized carbon quantum dots as fluorescent nanoprobe for determination of tetracyclines and cell imaging. *Mikrochim Acta*. 2020;187(6):1–10. doi:10.1007/s00604-020-04328-1
3. Meziani MJ, Dong X, Zhu L, et al. Visible-light-activated bactericidal functions of carbon "quantum" dots. *ACS Appl Mater Interfaces*. 2016;8(17):10761–10766. doi:10.1021/acsami.6b01765
4. Liu H, Lv X, Qian J, et al. Graphitic carbon nitride quantum dots embedded in carbon nanosheets for near-infrared imaging-guided combined photo-chemotherapy. *ACS Nano*. 2020;14(10):13304–13315. doi:10.1021/acsnano.0c05143
5. Mazumdar A, Haddad Y, Milosavljevic V, et al. Peptide-carbon quantum dots conjugate, derived from human retinoic acid receptor responder protein 2, against antibiotic-resistant gram positive and gram negative pathogenic bacteria. *Nanomaterials (Basel)*. 2020;10(2):325. doi:10.3390/nano10020325
6. Ran HH, Cheng X, Bao YW, et al. Multifunctional quaternized carbon dots with enhanced biofilm penetration and eradication efficiencies. *J Mater Chem B*. 2019;7(33):5104–5114. doi:10.1039/C9TB00681H
7. Yang J, Zhang X, Ma YH, et al. Carbon dot-based platform for simultaneous bacterial distinguishment and antibacterial applications. *ACS Appl Mater Interfaces*. 2016;8(47):32170–32181. doi:10.1021/acsami.6b10398
8. Yang J, Gao G, Zhang X, Ma Y-H, Chen X, Wu F-G. One-step synthesis of carbon dots with bacterial contact-enhanced fluorescence emission: fast Gram-type identification and selective Gram-positive bacterial inactivation. *Carbon*. 2019;146:827–839. doi:10.1016/j.carbon.2019.02.040
9. Bajpai VK, Khan I, Shukla S, et al. Multifunctional N-P-doped carbon dots for regulation of apoptosis and autophagy in B16F10 melanoma cancer cells and in vitro imaging applications. *Theranostics*. 2020;10(17):7841–7856. doi:10.7150/thno.42291
10. Li F, Li T, Sun C, Xia J, Jiao Y, Xu H. Selenium-doped carbon quantum dots for free-radical scavenging. *Angew Chem Int Ed Engl*. 2017;56(33):9910–9914. doi:10.1002/anie.201705989
11. Wang X, Zhang Y, Kong H, et al. Novel mulberry silkworm cocoon-derived carbon dots and their anti-inflammatory properties. *Artif Cells Nanomed Biotechnol*. 2020;48(1):68–76. doi:10.1080/21691401.2019.1699810
12. Wang X, Zhang Y, Zhang M, et al. Novel carbon dots derived from radix and their anti-gout effects. *Molecules*. 2019;24(22):4152. doi:10.3390/molecules24224152
13. Wang S, Zhang Y, Kong H, et al. Antihyperuricemic and anti-gouty arthritis activities of Aurantii fructus immaturus carbonisata-derived carbon dots. *Nanomedicine (Lond)*. 2019;14(22):2925–2939. doi:10.2217/nnm-2019-0255
14. Zhao Y, Zhang Y, Kong H, et al. Haemostatic nanoparticles-derived bioactivity of from carbonisata. *Molecules*. 2020;25(3):446. doi:10.3390/molecules25030446
15. Sun Z, Lu F, Cheng J, et al. Hypoglycemic bioactivity of novel eco-friendly carbon dots derived from traditional Chinese medicine. *J Biomed Nanotechnol*. 2018;14(12):2146–2155. doi:10.1166/jbn.2018.2653
16. Zhang M, Cheng J, Zhang Y, et al. Green synthesis of -based carbon dots attenuates chemical and thermal stimulus pain in mice. *Nanomedicine (Lond)*. 2020;15(9):851–869. doi:10.2217/nnm-2019-0369
17. Bi W-P, Man H-B, Man M-Q. Efficacy and safety of herbal medicines in treating gastric ulcer: a review. *World J Gastroenterol*. 2014;20(45):17020–17028. doi:10.3748/wjg.v20.i45.17020
18. Chiu PW. Endoscopic management of peptic ulcer bleeding: recent advances. *Clin Endosc*. 2019;52(5):416–418. doi:10.5946/ce.2018.182
19. Maes ML, Fixen DR, Linnebur SA. Adverse effects of proton-pump inhibitor use in older adults: a review of the evidence. *Ther Adv Drug Saf*. 2017;8(9):273–297. doi:10.1177/2042098617715381
20. Wilhelm SM, Rjater RG, Kale-Pradhan PB. Perils and pitfalls of long-term effects of proton pump inhibitors. *Expert Rev Clin Pharmacol*. 2013;6(4):443–451. doi:10.1586/17512433.2013.811206
21. Wang A, Yerxa J, Agarwal S, et al. Surgical management of peptic ulcer disease. *Curr Probl Surg*. 2020;57(2):100728.
22. Abd El Hady WE, Mohamed EA, Soliman O-AE-A, El-Sabbagh HM. In vitro-in vivo evaluation of chitosan-PLGA nanoparticles for potentiated gastric retention and anti-ulcer activity of diosmin. *Int J Nanomedicine*. 2019;14:7191–7213. doi:10.2147/IJN.S213836
23. El-Batal AI, Ahmed SF. Therapeutic effect of Aloe vera and silver nanoparticles on acid-induced oral ulcer in gamma-irradiated mice. *Braz Oral Res*. 2018;32:e004. doi:10.1590/1807-3107bor-2018.vol32.0004

24. Liu X, Wang Y, Yan X, et al. Novel Phellodendri Cortex (Huang Bo)-derived carbon dots and their hemostatic effect. *Nanomedicine (Lond)*. 2018;13(4):391–405. doi:10.2217/nnm-2017-0297
25. Xue Z, Shi G, Fang Y, et al. Protective effect of polysaccharides from Radix Hedysari on gastric ulcers induced by acetic acid in rats. *Food Funct*. 2019;10(7):3965–3976. doi:10.1039/C9FO00433E
26. Mousa AM, El-Sammad NM, Hassan SK, et al. Antiulcerogenic effect of Cuphea ignea extract against ethanol-induced gastric ulcer in rats. *BMC Complement Altern Med*. 2019;19(1):345. doi:10.1186/s12906-019-2760-9
27. Gao R, Wu Z, Wang L, et al. Green preparation of fluorescent nitrogen-doped carbon quantum dots for sensitive detection of oxytetracycline in environmental samples. *Nanomaterials (Basel)*. 2020;10(8):1561. doi:10.3390/nano10081561
28. Cheng C, Shi Y, Li M, Xing M, Wu Q. Carbon quantum dots from carbonized walnut shells: structural evolution, fluorescence characteristics, and intracellular bioimaging. *Mater Sci Eng C Mater Biol Appl*. 2017;79:473–480. doi:10.1016/j.msec.2017.05.094
29. Balan WS, Janaun J, Chung CH, et al. Esterification of residual palm oil using solid acid catalyst derived from rice husk. *J Hazard Mater*. 2020;404(Pt B):124092. doi:10.1016/j.jhazmat.2020.124092
30. Atchudan R, Edison T, Mani S, et al. Facile synthesis of a novel nitrogen-doped carbon dot adorned zinc oxide composite for photodegradation of methylene blue. *Dalton Trans*. 2020;49(48):17725–17736. doi:10.1039/D0DT02756A
31. Yang R, Guo X, Jia L, Zhang Y, Zhao Z, Lonshakov F. Green preparation of carbon dots with mangosteen pulp for the selective detection of Fe3+ ions and cell imaging. *Appl Surf Sci*. 2017;423:426–432. doi:10.1016/j.apsusc.2017.05.252
32. Wei X, Li L, Liu J, et al. Green synthesis of fluorescent carbon dots from gynostemma for bioimaging and antioxidant in zebrafish. *ACS Appl Mater Interfaces*. 2019;11(10):9832–9840. doi:10.1021/acsami.9b00074
33. Muhammad W, Ullah N, Haroon M, Abbasi BH. Optical, morphological and biological analysis of zinc oxide nanoparticles (ZnO NPs) using Papaver somniferum L. *RSC Adv*. 2019;9(51):29541–29548. doi:10.1039/C9RA04424H
34. Atchudan R, Edison TNJI, Chakradhar D, Perumal S, Shim -J-J, Lee YR. Facile green synthesis of nitrogen-doped carbon dots using Chionanthus retusus fruit extract and investigation of their suitability for metal ion sensing and biological applications. *Sens Actuators B Chem*. 2017;246:497–509. doi:10.1016/j.snb.2017.02.119
35. Chen Y, Niu Y, Tian T, et al. Microbial reduction of graphene oxide by Azotobacter chroococcum. *Chem Phys Lett*. 2017;677:143–147. doi:10.1016/j.cplett.2017.04.002
36. Manchala S, Gandamalla A, Vempuluru NR, Muthukonda Venkatakrishnan S, Shanker V. High potential and robust ternary LaFeO3/CdS/carbon quantum dots nanocomposite for photocatalytic H2 evolution under sunlight illumination. *J Colloid Interface Sci*. 2021;583:255–266. doi:10.1016/j.jcis.2020.08.125
37. Zhang XD, Li J, Niu JN, Bao XP, Zhao HD, Tan M. Fluorescent carbon dots derived from urine and their application for bio-imaging. *Methods*. 2019;168:84–93. doi:10.1016/j.ymeth.2019.04.005
38. Chen X, Wang X, Cao G, et al. Colorimetric and fluorescent dual-identification of glutathione based on its inhibition on the 3D ball-flower shaped Cu-hemin-MOF's peroxidase-like activity. *Mikrochim Acta*. 2020;187(11):601. doi:10.1007/s00604-020-04565-4
39. Ke C-B, Lu T-L, Chen J-L. Excitation-independent dual emissions of carbon dots synthesized by plasma irradiation of ionic liquids: ratiometric fluorometric determination of norfloxacin and mercury(II). *Microchimica Acta*. 2019;186(6):376. doi:10.1007/s00604-019-3505-7
40. Long R, Tang C, Li T, et al. Dual-emissive carbon dots for dual-channel ratiometric fluorometric determination of pH and mercury ion and intracellular imaging. *Mikrochim Acta*. 2020;187(5):307. doi:10.1007/s00604-020-04287-7
41. Wu D, Li BL, Zhao Q, et al. Assembling defined DNA nanostructure with nitrogen-enriched carbon dots for theranostic cancer applications. *Small*. 2020;16(19):e1906975. doi:10.1002/smll.201906975
42. Li C, Qin Z, Wang M, Liu W, Jiang H, Wang X. Manganese oxide doped carbon dots for temperature-responsive biosensing and target bioimaging. *Anal Chim Acta*. 2020;1104:125–131. doi:10.1016/j.aca.2020.01.001
43. Qin YT, Feng YS, Ma YJ, He XW, Li WY, Zhang YK. Tumor-sensitive biodegradable nanoparticles of molecularly imprinted polymer-stabilized fluorescent zeolitic imidazolate framework-8 for targeted imaging and drug delivery. *ACS Appl Mater Interfaces*. 2020;12(22):24585–24598. doi:10.1021/acsami.0c05154
44. Yao H, Li J, Song Y, et al. Synthesis of ginsenoside re-based carbon dots applied for bioimaging and effective inhibition of cancer cells. *Int J Nanomedicine*. 2018;13:6249–6264. doi:10.2147/IJN.S176176
45. Liu J, Lu S, Tang Q, et al. One-step hydrothermal synthesis of photoluminescent carbon nanodots with selective antibacterial activity against Porphyromonas gingivalis. *Nanoscale*. 2017;9(21):7135–7142. doi:10.1039/C7NR02128C
46. Tong T, Hu H, Zhou J, et al. Glycyrrhizic-acid-based carbon dots with high antiviral activity by multisite inhibition mechanisms. *Small*. 2020;16(13):1–10.
47. Yan X, Zhao Y, Luo J, et al. Hemostatic bioactivity of novel Pollen Typhae Carbonisata-derived carbon quantum dots. *J Nanobiotechnology*. 2017;15(1):60. doi:10.1186/s12951-017-0296-z
48. Wang YZ, Kong H, Liu XM, et al. Novel carbon dots derived from cirsii japonici herba carbonisata and their haemostatic effect. *J Biomed Nanotechnol*. 2018;14(9):1635–1644. doi:10.1166/jbn.2018.2613
49. Cheng J, Zhang M, Sun Z, et al. Hemostatic and hepatoprotective bioactivity of Junci Medulla Carbonisata-derived carbon dots. *Nanomedicine (Lond)*. 2019;14(4):431–446. doi:10.2217/nnm-2018-0285
50. Wu J, Zhang M, Cheng J, et al. Effect of Lonicerae japonicae flos carbonisata-derived carbon dots on rat models of fever and hypothermia induced by lipopolysaccharide. *Int J Nanomedicine*. 2020;15:4139–4149. doi:10.2147/IJN.S248467
51. Fu Y, Wu HQ, Cui HL, Li YY, Li CZ. Gastroprotective and anti-ulcer effects of oxymatrine against several gastric ulcer models in rats: possible roles of antioxidant, antiinflammatory, and prosurvival mechanisms. *Phytother Res*. 2018;32(10):2047–2058. doi:10.1002/ptr.6148
52. Hoesel B, Schmid JA. The complexity of NF-kappaB signaling in inflammation and cancer. *Mol Cancer*. 2013;12:86. doi:10.1186/1476-4598-12-86
53. Aziz RS, Siddiqua A, Shahzad M, Shabbir A, Naseem N. Oxyresveratrol ameliorates ethanol-induced gastric ulcer via down-regulation of IL-6, TNF-alpha, NF-kB, and COX-2 levels, and up-regulation of TFF-2 levels. *Biomed Pharmacother*. 2019;110:554–560. doi:10.1016/j.biopha.2018.12.002
54. Arab HH, Salama SA, Eid AH, Kabel AM, Shahin NN. Targeting MAPKs, NF-kappaB, and PI3K/AKT pathways by methyl palmitate ameliorates ethanol-induced gastric mucosal injury in rats. *J Cell Physiol*. 2019;234(12):22424–22438. doi:10.1002/jcp.28807
55. Yeo D, Hwang SJ, Kim WJ, Youn HJ, Lee HJ. The aqueous extract from Artemisia capillaris inhibits acute gastric mucosal injury by inhibition of ROS and NF-kB. *Biomed Pharmacother*. 2018;99:681–687. doi:10.1016/j.biopha.2018.01.118
56. Tahir M, Rahman MA, Khushtar M. Gastroprotective effect of Hyssopus officinalis L. leaves via reduction of oxidative stress in indomethacin-induced gastric ulcer in experimental rats. *Drug Chem Toxicol*. 2019;1–10. doi:10.1080/01480545.2019.1685537
57. Minatel IO, Francisqueti FV, Correa CR, Lima GP. Antioxidant activity of gamma-oryzanol: a complex network of interactions. *Int J Mol Sci*. 2016;17(8):1107. doi:10.3390/ijms17081107
58. Mahmoud YI, Abd El-Ghffar EA. Spirulina ameliorates aspirin-induced gastric ulcer in albino mice by alleviating oxidative stress and inflammation. *Biomed Pharmacother*. 2019;109:314–321. doi:10.1016/j.biopha.2018.10.118

59. Shi R, Dai X, Li W, et al. Hydroxyl-group-dominated graphite dots reshape laser desorption/ionization mass spectrometry for small biomolecular analysis and imaging. *ACS Nano*. 2017;11(9):9500–9513. doi:10.1021/acsnano.7b05328
60. Kelarakis A. Graphene quantum dots: in the crossroad of graphene, quantum dots and carbogenic nanoparticles. *Curr Opin Colloid*. 2015;20(5–6):354–361. doi:10.1016/j.cocis.2015.11.001
61. Abu Rabe DI, Al Awak MM, Yang F, et al. The dominant role of surface functionalization in carbon dots' photo-activated antibacterial activity. *Int J Nanomedicine*. 2019;14:2655–2665.
62. Ayaz F, Alas MO, Genc R. Differential immunomodulatory effect of carbon dots influenced by the type of surface passivation agent. *Inflammation*. 2020;43(2):777–783. doi:10.1007/s10753-019-01165-0
63. Xu X, Zhang K, Zhao L, et al. Aspirin-based carbon dots, a good biocompatibility of material applied for bioimaging and anti-inflammation. *ACS Appl Mater Interfaces*. 2016;8(48):32706–32716. doi:10.1021/acsami.6b12252
64. Qu Z, Liu L, Sun T, et al. Synthesis of bifunctional carbon quantum dots for bioimaging and anti-inflammation. *Nanotechnology*. 2020;31(17):175102. doi:10.1088/1361-6528/ab6b9d
65. Satoh K, Yoshino J, Akamatsu T, et al. Evidence-based clinical practice guidelines for peptic ulcer disease 2015. *J Gastroenterol*. 2016;51(3):177–194. doi:10.1007/s00535-016-1166-4
66. Sierra F, Suarez M, Rey M, Vela MF. Systematic review: proton pump inhibitor-associated acute interstitial nephritis. *Aliment Pharm Ther*. 2007;26(4):545–553. doi:10.1111/j.1365-2036.2007.03407.x
67. Aggarwal N. Drug-induced subacute cutaneous lupus erythematosus associated with proton pump inhibitors. *Drugs Real World Outcomes*. 2016;3(2):145–154. doi:10.1007/s40801-016-0067-4
68. Ho PM, Maddox TM, Wang L, et al. Risk of adverse outcomes associated with concomitant use of clopidogrel and proton pump inhibitors following acute coronary syndrome. *JAMA*. 2009;301(9):937–944. doi:10.1001/jama.2009.261
69. O'Donoghue ML, Braunwald E, Antman EM, et al. Pharmacodynamic effect and clinical efficacy of clopidogrel and prasugrel with or without a proton-pump inhibitor: an analysis of two randomised trials. *Lancet*. 2009;374(9694):989–997. doi:10.1016/S0140-6736(09)61525-7
70. Bajaj JS, Heuman DM, Hylemon PB, et al. Altered profile of human gut microbiome is associated with cirrhosis and its complications. *J Hepatol*. 2014;60(5):940–947. doi:10.1016/j.jhep.2013.12.019